Journal Pre-proofs

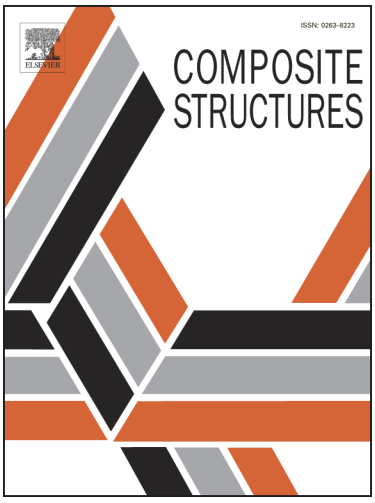

Simultaneous reinforcement of both rigidity and energy absorption of polyamide-based composites with hybrid continuous fibers by 3D printing

Kui Wang, Shixian Li, Yiyun Wu, Yanni Rao, Yong Peng

PII: S0263-8223(21)00315-9
DOI: https://doi.org/10.1016/j.compstruct.2021.113854
Reference: COST 113854

To appear in: *Composite Structures*

Received Date: 18 August 2020
Revised Date: 3 February 2021
Accepted Date: 13 March 2021

Please cite this article as: Wang, K., Li, S., Wu, Y., Rao, Y., Peng, Y., Simultaneous reinforcement of both rigidity and energy absorption of polyamide-based composites with hybrid continuous fibers by 3D printing, *Composite Structures* (2021), doi: https://doi.org/10.1016/j.compstruct.2021.113854

Simultaneous reinforcement of both rigidity and energy absorption of polyamide-based composites with hybrid continuous fibers by 3D printing

Kui Wang[1,2,3], Shixian Li[1,2], Yiyun Wu[1,4], Yanni Rao[1,2], Yong Peng[1,2,3]*

[1] Key Laboratory of Traffic Safety on Track of Ministry of Education, School of Traffic & Transportation Engineering, Central South University, Changsha, 410075, China

[2] Joint International Research Laboratory of Key Technology for Rail Traffic Safety, Central South University, Changsha, 410075, China

[3] National & Local Joint Engineering Research Center of Safety Technology for Rail Vehicle, Central South University, Changsha, 410075, China

[4] Department of mechanical engineering, University of Aveiro, Aveiro, 3810-193, Portugal

* Corresponding author e-mail address: yong_peng@csu.edu.cn

Abstract: The use of continuous fiber as reinforcement is well known to improve the mechanical performance of thermoplastic printed laminated composites. However, it is difficult to optimize the rigidity and energy absorption of continuous fiber reinforced composite components, since the inherent conflict between strength and ductility. For this purpose, this study focused on the design and characterization of continuous fibers reinforced polyamide (PA)-based composites, prepared via 3D printing, with synergistic enhancement of the strength and ductility. Continuous carbon and Kevlar fibers were used as reinforcements for production of printed non-hybrid and hybrid composites. The quasi-static indentation (QSI) test and structural evolutions analysis of composites were conducted to evaluate the mechanical properties and reveal the deformation and failure mechanisms. A Volume Average Stiffness (VAS) model and a hybrid effect model were introduced to predict the effective stiffness and to analyze the hybrid effect on the energy absorption capabilities of the printed hybrid composites, respectively. The results showed that the

addition of the continuous carbon and Kevlar fibers with a certain designed improved toughness of the composite, which led to an enhancement of the energy absorption properties. The deformation and failure mechanisms of hybrid continuous fiber reinforced composites highly depended on the designed position of fibers. For the printed hybrid composites, the highest indentation force could be achieved when continuous Kevlar fiber layers were placed at the rear side. While the highest energy absorption capability of the printed composites was captured when continuous carbon fiber layers were positioned at the rear side.

Keywords: 3D printing; continuous carbon fiber; continuous Kevlar fiber; quasi-static indentation test; hybrid effect; VAS modelling.

1 Introduction

3D printing, also known as additive manufacturing (AM), is one of the most promising techniques for fabricating objects with complex structures. AM technology for polymers and polymer composites forming is a broad term encompassing stereolithography apparatus (SLA) technique for photopolymer liquid [1], fused deposition modeling (FDM) for polymer filaments [2, 3], selective laser sintering (SLS) for polymer powders [4], and laminated object manufacturing (LOM) for polymer laminations [5]. Among these, 3D printing based on FDM approach is becoming popular due to its low-cost, simple operation, low material waste and environmental friendliness [6, 7].

Thermoplastic polymers, such as acrylonitrile butadiene styrene (ABS), polylactic acid (PLA) and polyamide (PA), are widely used in FDM due to their

convenience for parts fabrication and their availability [8-10]. Despite numerous printing polymers available, the stiffness and strength of these pristine thermoplastics are relatively weak for structural purposes [11, 12]. In recent years, continuous fibers, including carbon fibers (CFs), Kevlar fibers (KFs), and glass fibers (GFs), started to be used as reinforcements to improve the mechanical behaviors of thermoplastic-based composites by 3D printing. Van Der Klift et al. [13] evaluated the mechanical behaviors of nylon and continuous carbon fiber reinforced nylon composites manufactured by 3D printing. They concluded that the tensile strength of the composites increased significantly, while their ductility decreased due to the presence of the rigid continuous carbon fibers, indicating that the addition of continuous carbon fibers changed the failure mode of composites from ductility to brittleness. Heidari-Rarani et al. [14] studied the mechanical properties of 3D printed continuous carbon fiber reinforced PLA composites. They confirmed that the tensile and bending strengths of the composites increased up to 35% and 108% respectively, in comparison to pure PLA. However, the ductility of the PLA composites decreased significantly with the addition of the continuous carbon fiber. The increased tensile and bending strengths, and decreased ductility of PLA based composites were attributed to the presence of the more rigid but brittle continuous carbon fibers. Dickson et al. [15] assessed the mechanical responses of 3D printed continuous Kevlar fiber reinforced PA-based composites by three-points bending tests. The results showed that the toughness of continuous Kevlar fiber reinforced PA-based composites increased up to 48%, comparing to unreinforced PA. This was attributed

to the toughening effect provided by the presence of continuous Kevlar fibers. Brooks et al. [16] investigated the mechanical behaviors of continuous Kevlar fiber reinforced PLA-based composites by compressive tests. The results demonstrated that the introduction of the continuous Kevlar fiber clearly increased toughness of materials but reduced the composites compressive stiffness. The increased toughness was attributed to the addition of ductile continuous Kevlar fibers.

Therefore, it can be seen that the addition of single continuous fiber often increases some mechanical properties of composites, but at the same time decreases other mechanical behaviors [17]. However, for structure application, the balance of materials properties needs to be considered. To overcome the limitation caused by the presence of single fiber, composites manufacturing usually use hybrid concept, by combining two or more different fibers, in order to have the comprehensive performance improvement or designable mechanical properties. In the literature, the study of hybrid-reinforcement effect on the mechanical properties of composites was mainly focused on the inclusion-filled polymers or woven/non-woven fabrics prepared via traditional methods [18, 19]. The mechanical responses of hybrid short fiber-reinforced composites manufactured via 3D printing were partially studied [20]. For continuous fiber reinforced 3D printed composites, the simultaneously use of the multi-type of fibers with different properties could be an effective method to tailor the mechanical behaviors. However, to the best of our knowledge, no studies have been conducted to assess the mechanical responses of 3D printed hybrid continuous fiber reinforced composites. For these composites, the mechanical properties would not

only depend on the properties of each fiber but also on the interactions between the printed beads and layers [21]. As a result, it is essential to study the mechanical behaviors of 3D printed continuous hybrid fiber reinforced composites with underlying deformation and failure mechanisms.

In this paper, PA-based composites filled with non-hybrid and hybrid continuous carbon and Kevlar fibers were manufactured by 3D printing. The mechanical properties of the composites with different designs were evaluated by means of the quasi-static penetration investigations. The structural evolution of printed hybrid composites induced by strain was captured at multi-scales, in order to reveal the deformation and failure mechanisms with the effect of hybrid conception. A Volume Average Stiffness (VAS) model and a hybrid effect model were introduced to predict the effective stiffness and to analyze the hybrid effect on the energy absorption capabilities of the printed hybrid composites.

2 Experimental methodology

2.1 Materials and processing

In this study, three kinds of printing filament from MarkForged® were chosen. Short carbon fiber reinforced polyamide was used as effective matrix (onyx), continuous carbon fiber and continuous Kevlar fiber filaments were selected as reinforcement. The reinforced continuous fiber filaments were composed of continuous carbon or Kevlar fiber bundles infused with a large amount of thermoplastic PA sizing agent [22]. The continuous carbon fibers and continuous Kevlar fibers in filaments corresponded to 47.98 wt. % and 20.35 wt. %, respectively,

obtained by thermogravimetric analysis (TGA). Prior to use, the materials were stored in a dry box to minimize the humidity. 3D printed composites with continuous fibers were fabricated using a MarkForged® Mark7 3D printer. Fig. 1 (a) shows the diagram of the printing procedure, which consists of two modules, allowing the printing of different filaments independently. In the current study, the matrix and continuous fiber layers were printed with extrusion temperatures of 270 °C and 250 °C, respectively, onto a non-heated printing platform. The rectangular specimens with dimensions of 50.0 mm × 50.0 mm × 1.0 mm were prepared [23]. As shown in Fig. 1 (b), each specimen had a total of ten layers including four continuous fiber layers (continuous Kevlar fiber reinforced layers (CKFRLs) and continuous carbon fiber reinforced layers (CCFRLs)) and six matrix layers (short carbon fiber reinforced layers (SCFRLs)). The printing filament volume consumptions for each layer were estimated by the slicing software as listed in Table 1. Therefore, the volume fractions of printing continuous fiber filaments could be calculated. And the weight fractions (W_f) of continuous fiber filament could be obtained from the printed volume fractions (V_f) of continuous fiber filament using the following formula [24]:

$$V_f = \frac{W_f}{W_f + \frac{\rho_f}{\rho_m}(1 - W_f)} \quad (1)$$

where the continuous carbon fiber filament density is ρ_f = 1.4 g/cm3, the continuous Kevlar fiber filament density is ρ_f = 1.2 g/cm3, and the effective matrix filament density is ρ_m = 1.1 g/cm3 [22]. The weight fractions of continuous fibers then could be calculated using TGA results of the filaments. All the layers were printed with ±

45° deposition raster angles. In order to investigate the hybrid effect of continuous fibers on the mechanical properties of printed laminated composites, we changed the layer configuration by printing continuous carbon and Kevlar fibers at different positions as displayed in Fig. 1 (b). In the following denotation, "C" stands for long continuous carbon fiber strengthened polyimide, "K" for continuous Kevlar fibers reinforced polyimide. The composites in Fig. 1 were denoted as C-C, K-K, K-C and C-K. The composite with 10 layers of short carbon fiber reinforced polyamide was denoted as matrix as a control sample.

Table 1 Volume and weight fractions of continuous fibers

Specimens	Volume of printing filaments (cm^3)			Continuous fibers filaments volume fraction (vol. %)		Continuous fibers filaments weight fraction (wt. %)		Continuous fibers weight fraction (wt. %)	
	Matrix filaments	Continuous fiber filaments							
		Carbon	Kevlar	Carbon	Kevlar	Carbon	Kevlar	Carbon	Kevlar
C-C	2.04	1.08		34.61		40.21	-	19.29	-
K-K	2.04		0.90		30.61	-	32.48	-	6.61
C-K	2.04	0.54	0.45	17.82	14.85	21.63	15.98	10.38	3.25
K-C	2.04	0.54	0.45	17.82	14.85	21.63	15.98	10.38	3.25

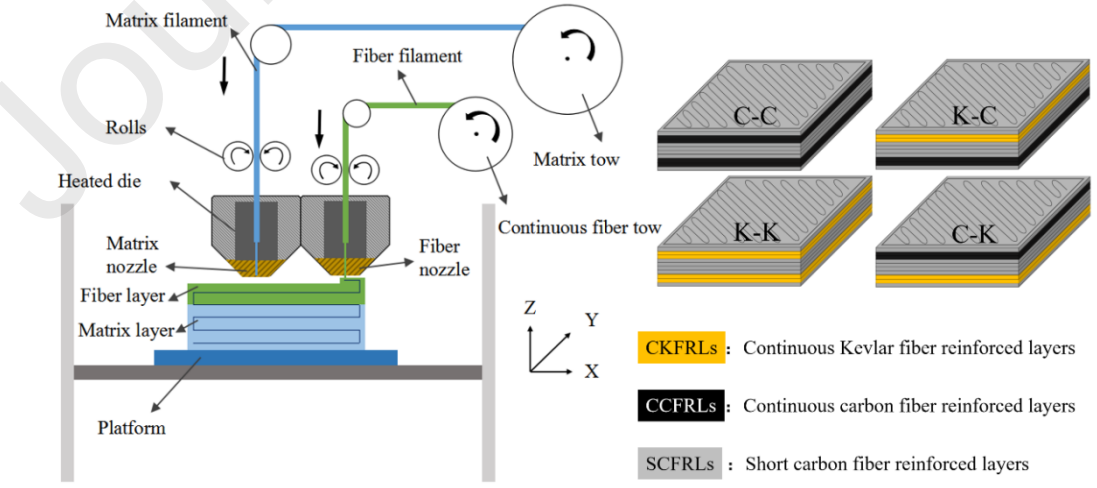

(a) (b)

Fig. 1. Schematic representation of (a) FDM process with continuous fibers, (b) configuration of printing specimens.

2.2 Characterization

The quasi-static indentation (QSI) tests in the current study were performed to investigate the mechanical responses including damage evolutions of the printed laminated composites by an MTS universal mechanical testing machine (E44, MTS Co., USA) with a 1 kN load cell. As shown in Fig.2, the tests were carried out with a custom-made fixture. It consisted of two plates, recognized as a thick section cover plate with a circular hole (Ds = 40 mm) in the middle and a support plate with a same circular hole. A hemispherical end punch (Dp = 10 mm) was used for the tests. After clamping the specimen, a cross-head indentation loading rate of 1.25 mm/min was applied, according to the ASTMD-6264 standard. All the specimens were loaded up to the complete perforation of the material. Since the mechanical properties of many composites are sensitive to environmental temperature, tests were carried out at room temperature. Three repeated tests were conducted for each composite configuration, and the average values were calculated with standard deviation.

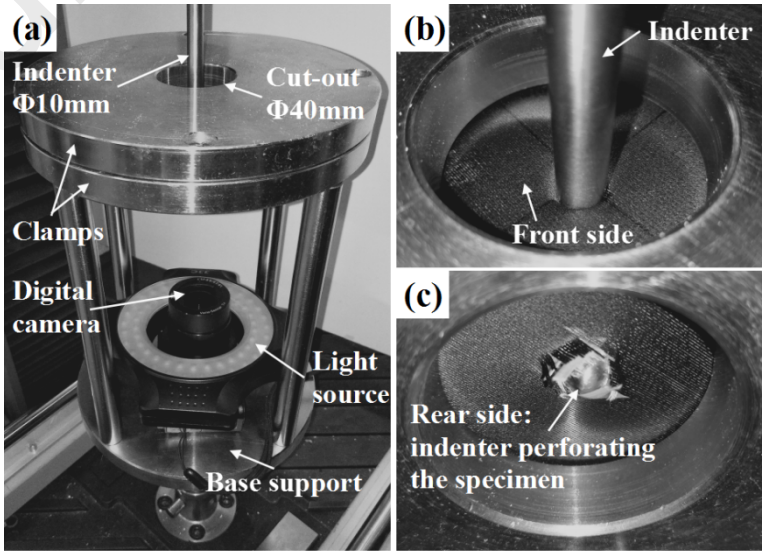

Fig. 2. (a) Quasi-static indentation test setup; (b) penetration of the front side; (c) perforation of the rear side.

3 Results and discussion

3.1 Mechanical behavior of the non-hybrid and hybrid composites

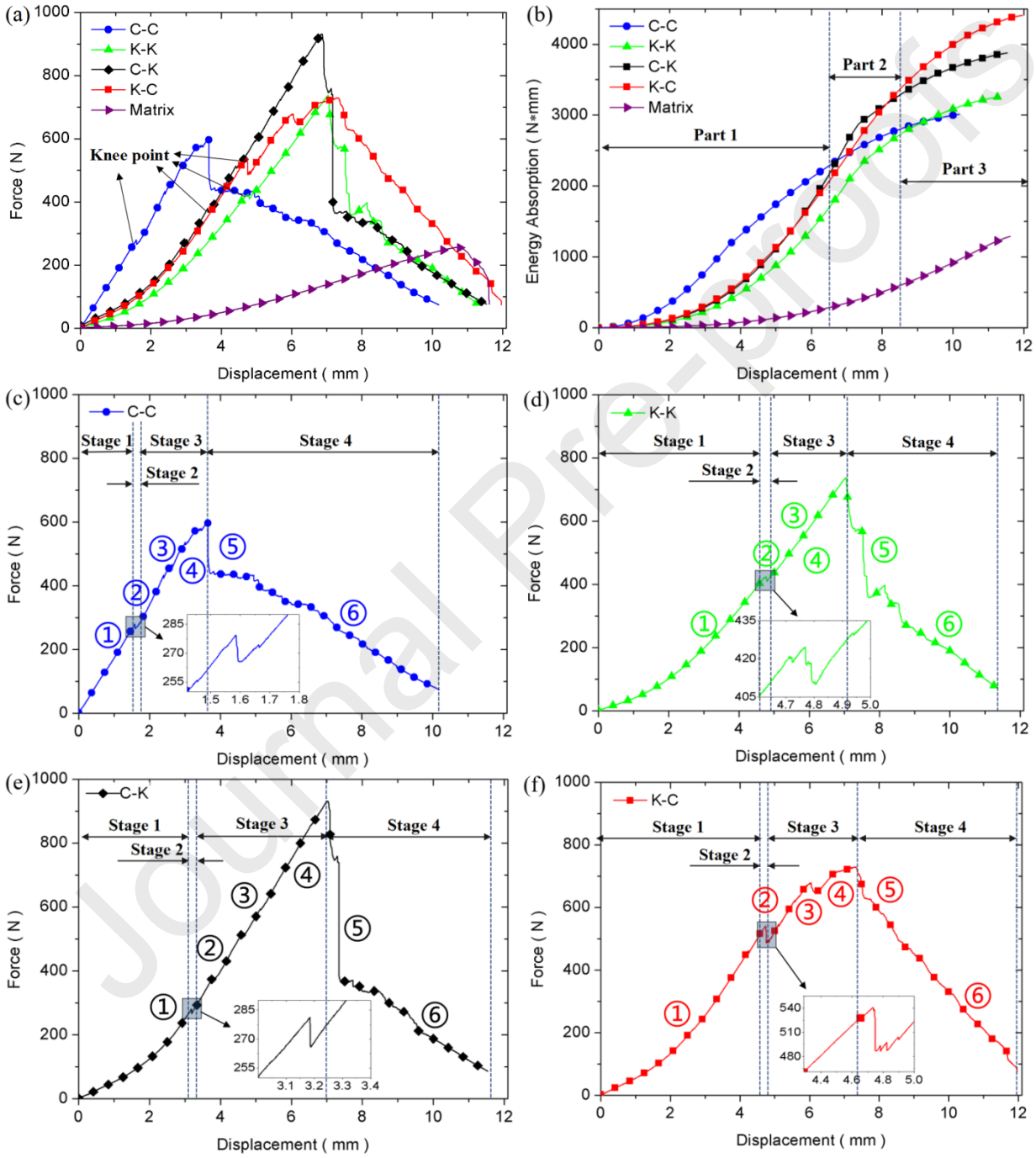

Fig. 3. Quasi-static indentation behaviors of printed non-hybrid and hybrid composites (a) Force-displacement curves,(b) energy-absorption displacement curves

and (c-f) summary of the damage evolutions (①Elastic response; ②Delamination onset and de-bonding between adjacent filaments ; ③Delamination propagation; ④Filaments breakage (matrix); ⑤Filaments breakage (fiber); ⑥Friction and perforation).

Table 2. Indentation results for non-hybrid and hybrid composites.

Composites	F_{max} **(N)**	$E_{absorbed}$ **(N*mm)**	**Disp. for max load (mm)**
Matrix	256.3 ± 10.3	1289.9 ± 8.1	10.7 ± 0.2
C-C	600.2 ± 17.9	3011.6 ± 146.1	3.6 ± 0.2
K-K	755.8 ± 59.9	3255.9 ± 109.2	7.1 ± 0.3
K-C	729.1 ± 35.2	4409.1 ± 67.7	7.2 ± 0.5
C-K	931.5 ± 23.4	3878.6 ± 100.8	6.8 ± 0.2

The load-displacement characteristics of the matrix, non-hybrid, and hybrid composites are shown in Fig. 3 (a). In this figure, for all the composites, the loads increased linearly with increasing displacement up to the first load drop (knee point). After this linear stage, the loads continued to increase as the displacement increased. Before arriving at the maximum loads, the force-displacement curves for C-C, C-K and K-C exhibited other small load drops after the first knee points. However, the load of K-K increased continuously without any drops between the first load drop and the maximum load as shown in Fig. 3 (a). Meanwhile, for C-C, the indentation force reached the maximum value at the displacement of 3.6 ± 0.2 mm, while the displacements of maximum load for K-K, K-C and C-K were 7.1 ± 0.3 mm, 7.2 ± 0.5 mm and 6.8 ± 0.2 mm, respectively (Table 2). It was noticed that, after each load drop,

the slopes of force-displacement curves for all composites decreased gradually till the maximum loads. And the initial average slope of C-C was much high than that of K-K, the slopes of C-K and K-C were closed. After the maximum loads, the forces of C-C, C-K and K-K dropped sharply, but the force of K-C decreased gently. In addition, different from the force-displacement behaviors of composites, the force of matrix increased slowly with increasing displacement, a maximum load of 256.3 ± 10.3 N was achieved at a displacement of 10.7± 0.2 mm (Fig. 3 (a) and Table 2).

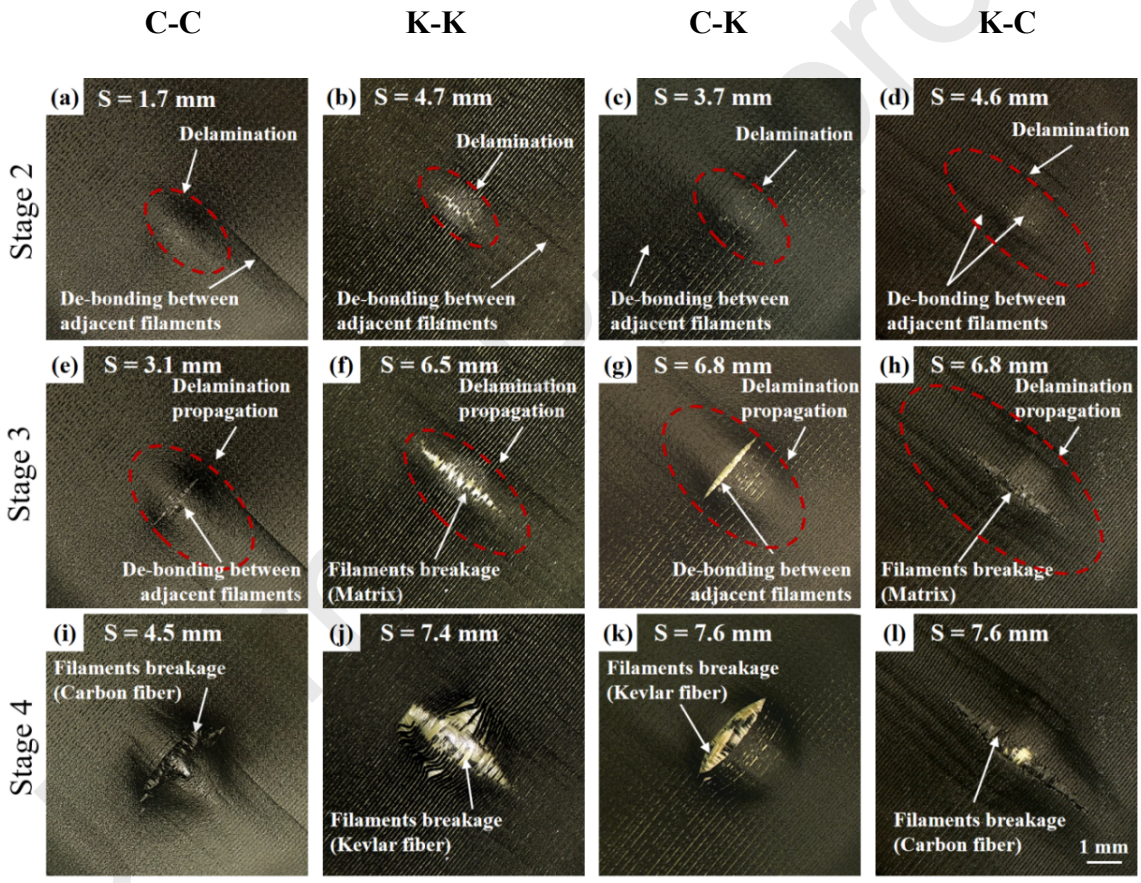

Fig. 4. Distal side graphs of (a) (e) (i) C-C, (b) (f) (j) K-K, (c) (g) (k) C-K and (d) (h) (l) K-C composites show the details of the damage evolutions and failure modes induced by quasi-static indentation.

The energy absorption capability of the composites could be represented by the area under the load-displacement curves. Fig. 3 (b) shows the energy absorption-displacement curves of all the specimens. The five curves were able to be divided into three parts by intersections. For the displacement range from 0 mm to 6.3 mm, the C-C showed the highest slope, representing higher energy absorption rate at relatively small displacement. The second part consisted the displacement range from 6.3 mm to 8.3 mm, and the mechanical behaviors of C-K in this range not only exhibited high rigidity but also high energy absorption capability (see Fig.4 (a) and (b)). Part 3 included the displacement range from 8.3 mm to 12 mm, and the K-C presented higher energy absorption capabilities within this stage.

The load-displacement curves of printed non-hybrid and hybrid composites could be divided into four stages according to the different deformation and failure mechanisms, as exhibited in Fig.3 (c-f). The corresponded structural evolutions and failures of the composites induced by indentation are shown in Fig.4. And Fig. 5 displays the damage behaviors of the composites after the quasi-static indentation tests from different views. In Fig.3 (c-f), the stage 1 corresponded to the elastic parts linked with the stiffness of the composites, covered the displacement ranges from 0.0 to 1.6 mm for C-C, from 0.0 to 4.7 mm for K-K, from 0.0 to 3.2 mm for C-K and from 0.0 to 4.8 mm for K-C, respectively. This stage could be associated with the increase of the indentation load according to the Hertzian contact and bending response, up to the first load drop. And the higher effective stiffness of C-C could be attributed to the presence of higher content of rigid continuous carbon fibers. In stage

2, the sudden slight load drops were observed at the displacements of 4.7 and 4.8 mm for K-K and K-C, as shown in Fig. 3 (d) and (f). However, for C-C and C-K, the load drops occurred earlier, captured at displacements of 1.6 mm and 3.2 mm (as shown in Fig. 3 (c) and (e). These small load drops could be attributed to the initiation of delamination as well as de-bonding between adjacent filaments in the bottom layers (Fig.4 (a-d)). The earlier load drops for C-C and C-K were probably due to the localized inter-layer fractures induced by the fragile carbon fibers placed in the upper layers of composites (Fig. 5 (a) and (d)). In Stage 3, the loads continued to increase with increasing displacement but with lower slopes than those for stage 1. These phenomena were probably attributed to the propagation of the delamination without significant crack propagation in thickness direction (Fig. 4 (e-h)). For C-C and C-K composites, the de-bonding propagation between matrix filaments were observed in the bottom of composites, which justified the small load drops in the load–displacement curves within this stage. For K-C composites, matrix filaments breakages were observed at bottom layers of composites (Fig. 4 (h)), causing in the largest loading drops in stage 3 among the four composites. However, although K-K exhibited similar matrix filaments breakages, its limited extension of delamination and the ductile Kevlar fibers kept the continuous increase of load within this stage (see Fig.5 (b)). For all the composites, the bottom part played an important role for load carrying. However, Kevlar fibers with high toughness at the bottom side of composites might offer an elevated resistance to bear the tensile stresses than carbon fibers, causing the higher maximum indentation force for C-K than that of K-C. The last stage 4 in Fig.3

(c-f) could be associated to the fiber breakage and perforation of the composites as shown in Fig. 5. During this stage, large load drops could be found in the load–displacement curves (Fig. 3 (c-f)). As exhibited in Fig. 5, fiber breakage was observed at both sides of the composites. The fiber filaments breakage of the upper part was mainly due to the compressive stresses, although the shear stresses induced by the contact between indenter and composite also contributed to this breakage. For the rear part of the composites, the fiber filaments breakage was due to the bending tension stresses, resulting in bulging and splitting. In addition, it was also observed that the delamination between layers in the bottom layers was more significant compared to that in the up layers. For instance, when continuous carbon fibers placed in the bottom layers, a significant delamination propagated along XOY plane of continuous carbon fiber layers was observed. This phenomenon was due to a brittle nature of carbon fibers as well as poor transverse stress between carbon fiber layers [24]. However, when continuous Kevlar fibers placed at the bottom side and carbon fibers placed in the top layers, a large number of delamination propagated along XOZ plane could be found. This phenomenon was due to the toughness behavior of Kevlar fibers which inhibiting the growth of inter-layer cracking along the filaments in XOY plane. The extensive damage was caused by the fact that the de-bonding between filaments easily propagated due to low Mode I fracture toughness, inducing relatively large delamination in the distal interface for composites. Larger delamination in bottom layers was plausibly caused by its lower Mode II fracture toughness in comparison to up layers. Therefore, the designed position of fibers for the 3D printed non-hybrid and

hybrid composites played an important role influencing the damage mechanism of the materials [25]. It was important to point out that within this stage, load dropped slowly for K-C rather than other composites which dropped sharply. This phenomenon was due to the fibers fractured slowly since the matrix filaments breakage at the rear side of K-C composites in the last stage.

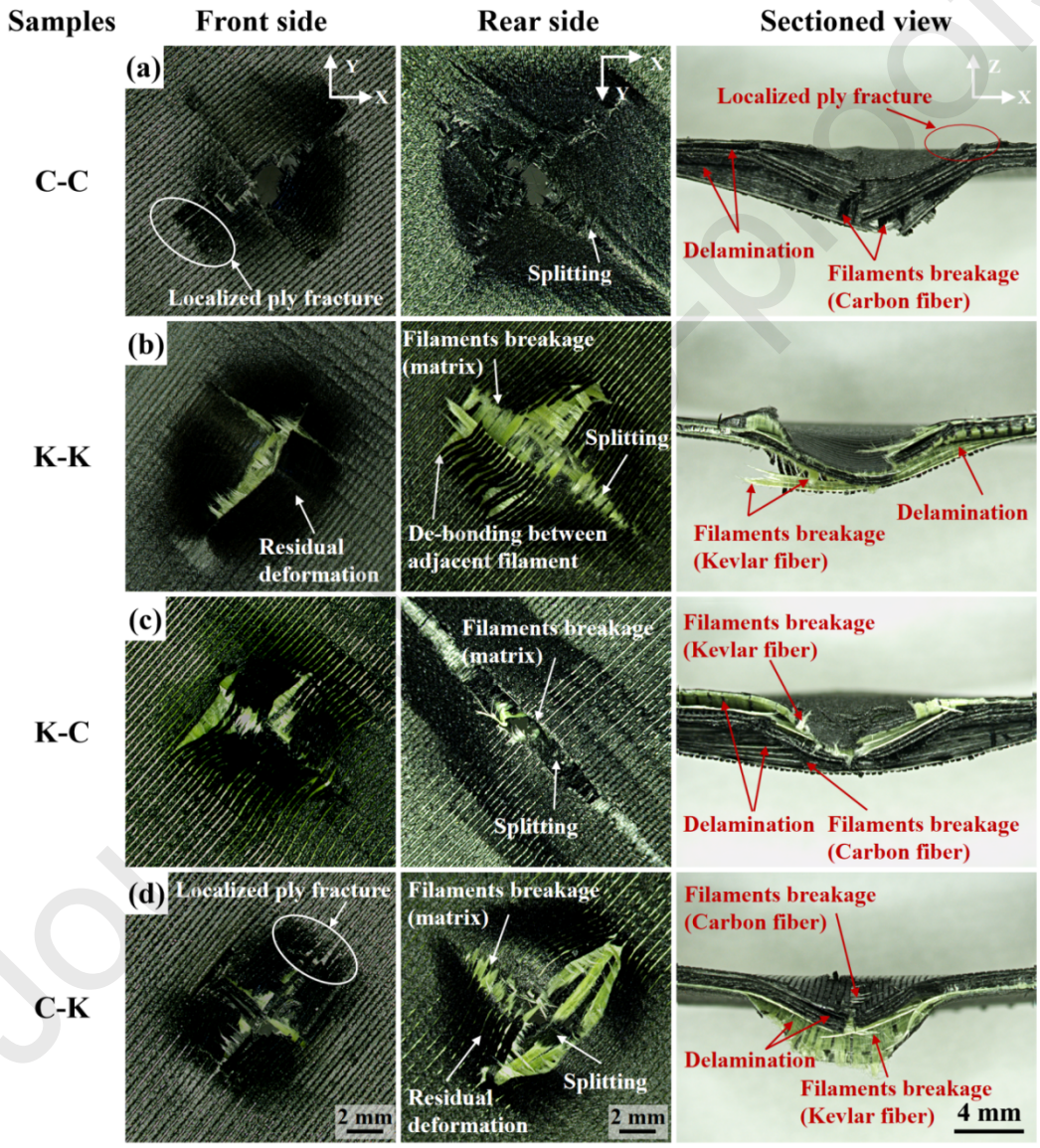

Fig. 5. Damaged sections of (a) C-C, (b) K-K, (c) K-C and (d) C-K composites.

The typical damage mechanisms of K-C composites were schematically shown

in Fig. 6. We chose K-C to show here because it exhibited the highest energy absorption capability in current investigation range (Fig.3 (b)), and other non-hybrid and hybrid composites displayed similar damage mechanisms. As shown in Fig. 6, during the QSI test, the de-bonding between adjacent filaments were first observed, accompanying with delamination of continuous fiber layers. At large indenter displacement, delamination propagated and followed by fiber breakages at the bottom layers. Eventually, fiber breakages occurred in all layers as the indenter perforated the specimens (Fig. 6).

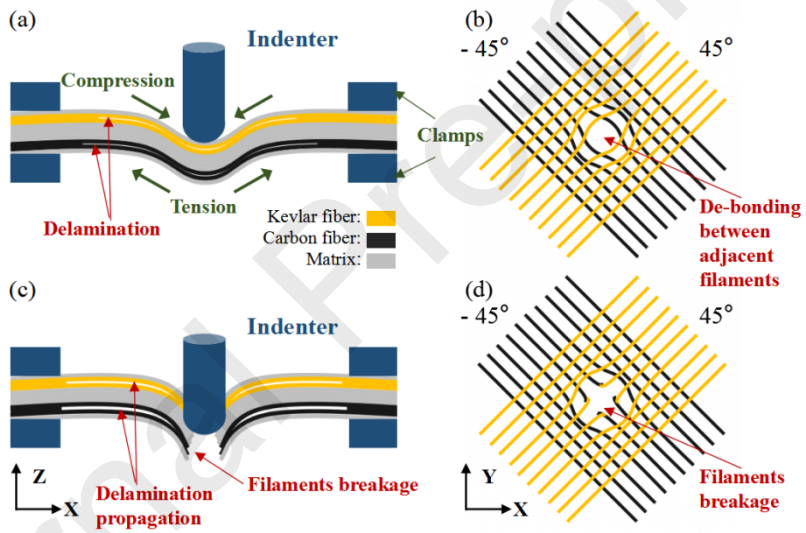

Fig. 6. Schematic presentation of damage mechanisms in 3D printed hybrid continuous fiber reinforced K-C composites.

In addition, fibers pull-out, fiber-matrix de-bonding, fibers breakage and delamination near the localized failure area were clearly observed by scanning electroscope machine (SEM) after QSI test, as shown in Fig.7 and Fig.8. The 3D printed continuous fiber reinforced non-hybrid and hybrid composites had different

kinds of interfaces between printed layers. Delamination between C-C and K-K interfaces was easily observed as shown in Fig. 7(a) (e) and in Fig. 8(a) (d). While, it seemed that C-O, K-O and O-O interfaces had less de-bonding problems compared to those of the C-C and K-K interfaces. These observed microscopic features could be used to explain that the lager delamination might cause higher energy absorption behavior [23]. In addition, examination of the fracture regions revealed that 'fibers pull-out' was a frequent occurrence failure mode for printed composites, with residual matrix remaining on the exposed fibers (Fig. 7(c) and (h)). Continuous Kevlar fibers (Fig. 7(h)) presented a plastic fractured surface with less residue on the fibers surface, suggesting a weaker bond to the matrix, comparing to that for carbon fibers (Fig. 7(c)). This conclusion was supported by the occurrence of inter-laminar failure, indicating that fibers were not consistently bonded to the matrix.

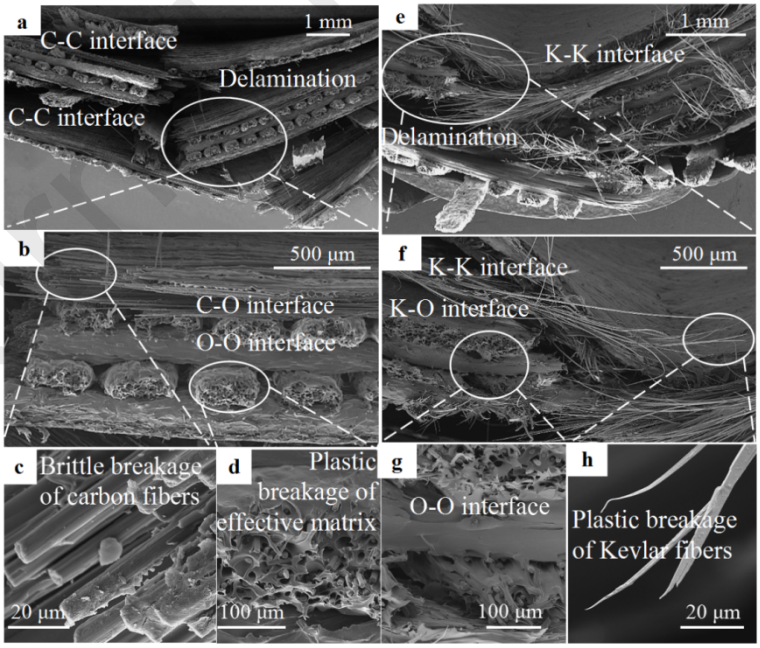

Fig. 7. SEM images of 3D printed non-hybrid (a)-(d) C-C and (e)-(h) K-K composites after QSI test

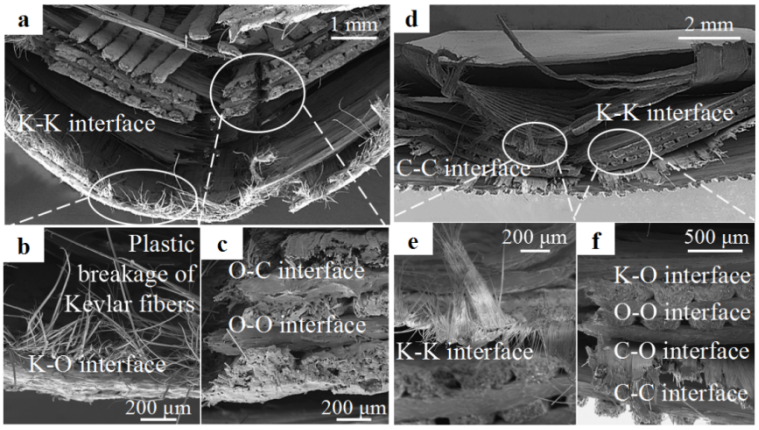

Fig. 8. SEM images of 3D printed hybrid (a)-(c) C-K and (d)-(f) K-C composites after QSI test

3.2 Analytical model of effective stiffness evaluation

In this investigation, an analytical model based on the volume average stiffness (VAS) method was used to predict the effective elastic properties of the continuous fiber reinforced 3D-printed non-hybrid and hybrid composites [26, 27]. Typical cross- sectional profile of the printed coupons is shown in Fig. 1(b). The section consisted of five regions formed by two or three types of materials, i.e. the carbon fibers or/and Kevlar fibers and effective matrix. Details of printed volume fraction for the composites are given in Table 1. The mechanical properties of the two considered types of fibers (Carbon and Kevlar) and effective matrix (Onyx) are given in Table 3. The volume fraction of each material component consumed to print a specimen can be estimated from the following equations:

$$V_{matrix} = \frac{V_{matrix}}{V_{matrix} + V_{fiber}} \tag{2}$$

$$V_{fiber} = \frac{V_{fiber}}{V_{matrix} + V_{fiber}} \tag{3}$$

where V_{matrix} and V_{fiber} were the volume fractions for the matrix and the considered continuous fibers (Carbon or/and Kevlar), respectively. The stiffness of the composites, Q, was calculated based on the stiffness of matrix and continuous fiber as follows:

$$Q = V_{matrix}\overline{Q}_{matrix} + V_{fiber}\overline{Q}_{fiber} \quad (4)$$

where Q_{matrix} and Q_{fiber} were respectively the stiffness of matrix and fibers in the global coordinate system which were related to Q_{matrix} and Q_{fiber} in the fiber coordinate systems as：

$$\overline{Q}_{matrix} = [T]^T Q_{matrix}[T] \quad (5)$$

$$\overline{Q}_{fiber} = [T]^T Q_{fiber}[T] \quad (6)$$

here, the stiffness of the matrix Q_{matrix}, the stiffness of fibers Q_{fiber} and transformation matrix [T] were defined as follows [26]:

$$Q_{matrix} = \begin{bmatrix} \frac{E}{1-\nu^2} & \frac{\nu E}{1-\nu^2} & 0 \\ \frac{\nu E}{1-\nu^2} & \frac{E}{1-\nu^2} & 0 \\ 0 & 0 & G \end{bmatrix} \quad (7)$$

$$Q_{fiber} = \begin{bmatrix} \frac{E_1}{1-\nu_{12}\nu_{21}} & \frac{\nu_{12}E_2}{1-\nu_{12}\nu_{21}} & 0 \\ \frac{\nu_{12}E_2}{1-\nu_{12}\nu_{21}} & \frac{E_2}{1-\nu_{12}\nu_{21}} & 0 \\ 0 & 0 & G_{12} \end{bmatrix} \quad (8)$$

$$[T] = \begin{bmatrix} cos^2\theta & sin^2\theta & sin\theta cos\theta \\ sin^2\theta & cos^2\theta & -sin\theta cos\theta \\ sin\theta cos\theta & -sin\theta cos\theta & cos^2\theta - sin^2\theta \end{bmatrix} \quad (9)$$

here, θ was the angle of matrix and fibers; E, G and ν were respectively the elastic modulus, shear modulus and Poisson's ratio of the matrix; and E_1, E_2, G_{12}, ν_{12}

were respectively the elastic modulus, shear modulus and Poisson's ratio of fibers. The effective elastic modulus, $E_{effective}$, and Poisson's ratio of the composites can be obtained from the components of the compliance matrix [S] as:

$$E_{effective} = \frac{1}{S_{11}} \tag{10}$$

where S_{11} was the components of the compliance matrix [S] which was the inversion of the stiffness matrix [Q] given in Eq. (3). The analytical effective stiffness was calculated by the expression as [28]:

$$K = \frac{E_{effective} h^3}{\mu b^2} \tag{11}$$

here, h and b were the thickness and the characteristic dimension of the laminate composites. μ = 0.175 was a correction factor which depends on the aspect ratio of the laminates [29].

Table 3 Adopted elastic properties of each component for the printed materials [26]

Material Properties	**Carbon**	**Kevlar**	**Effective matrix**
Longitudinal elastic modulus –E_1 (MPa)	85,000	30,000	1,440
Transvers elastic modulus –E_2 (MPa)	2,7000	10,000	1,440
In-plane shear modulus –G_{12}andG_{23} (MPa)	5000	5000	141
Poisson's ratio –ν_{12}	0.3	0.2	0.35

Table 4 presents a comparison of effective stiffness obtained from the analytical VAS model and experimental results. It can be seen that the effective stiffness for K-K, K-C and C-K were found to be predicted in high accuracy with differences of 3.9 %, 1.3 % and 2.7 %, respectively. However, the difference in the effective stiffness for C-C was higher than that of other composites being 8.5 %. This variation

could be attributed to the different actual contents of the carbon and Kevlar fiber in filaments (see 2.1 section), and the contents of carbon fiber were approximately 2 times higher than that of Kevlar fibers. This might explain the underestimation (8.5%) for C-C specimens.

Table 4 Comparison of measured and predicted effective stiffness

Composites	Predicted stiffness (N/mm)	Exp. stiffness (N/mm)	Difference (%)
K-K	29.08	30.27	3.9
C-C	159.30	174.13	8.5
K-C	53.40	52.70	1.3
C-K	53.40	54.86	2.7

3.3 Hybrid effect

Hybridization using different reinforcements is one of the effective ways to increase penetration resistance and energy absorption capability of the composites. By tailoring the filler, matrix and structural parameters, it is possible to control and design the hybrid composites with balanced or specific properties. A positive or negative hybrid effect for composites could be achieved according to their compositions by the rule of mixture (RoM) [30, 31].

Present study handled the absorbed energies of the printed composites to investigate the variation of hybrid effect by performing the rule of mixture. The resulting degree of hybrid effect (h_e) was calculated from Eq. (12) and (13).

$$E_{(RoM)} = \frac{1}{2}(E_{C-C} + E_{K-K}) \quad (12)$$

here, the E_{C-C} and E_{K-K} are the absorbed energy values through the indentation of non-hybrid composites (C-C and K-K composites). $E_{(RoM)}$ indicates the resulting rule of mixture values of absorbed energy for non-hybrid composites.

$$h_e = \frac{E_h}{E_{(RoM)}} - 1 \tag{13}$$

where Eh is the absorbed energy value of the hybrid composite. A positive or negative hybrid effect could be obtained according to Eq. (13).

$$\begin{aligned} &h_e > 0, \text{Positive hybrid effect} \\ &h_e < 0, \text{Negative hybrid effect} \end{aligned} \tag{14}$$

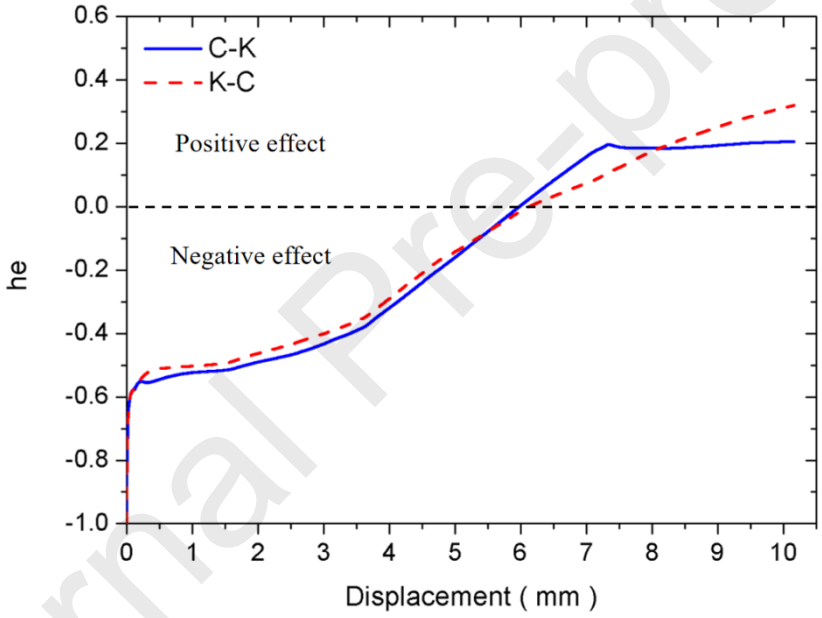

Fig. 9. The hybrid effect of the printed composites as function of indentation displacement

The hybrid effect of the printed composites as function of indentation displacement is shown in Fig. 9. In this figure, the hybrid C-K and K-C composites presented a positive hybrid effect after the indentation displacements of 5.7 mm, while displayed a negative effect from 0 mm to 5.7 mm. At relatively small

displacement, the negative hybrid effect of the composites was due to the significantly higher energy absorption rate of C-C rather than that of K-K (see Fig.3 (b)). By contrast, the positive hybrid effect of the composites was attributed to the higher energy absorption capabilities of C-K and K-C at large displacement. Besides, h_e $(K-C)$was higher than $h_e(C-K)$ in the end of the tests, which was attributed the stacking sequence of the continuous fibers in the lamina, effecting the force and displacement behaviors of the structure. More specifically, when carbon fibers were placed at the rear side and Kevlar fibers were placed at the front side, carbon fibers restricted the global deformation of the laminate due to high tensile strength and stiffness of the carbon fibers, resulting in increasing load carrying capacity of the composites [30].

4.Conclusions

In this work, we studied the mechanical responses of 3D printed PA-based non-hybrid and hybrid composite specimens using two different continuous fiber reinforcements (carbon and Kevlar fiber). The quasi-static indentation (QSI) tests were conducted to investigate the mechanical responses including damage evolution of the 3D printed laminated composites. The morphological structure changes at different indented displacements were determined by digital camera and scanning electron microscopy (SEM), in order to reveal the deformation and failure mechanisms of composites. A Volume Average Stiffness (VAS) model and a hybrid effect model were introduced to predict the effective stiffness and to analyze the

hybrid effect on the energy absorption capabilities of the printed hybrid composites.

It was found that the introduction of continuous carbon fibers increased the stiffness but decreased the ultimate failure displacements of the composites. However, the addition of continuous Kevlar fibers increased the ductility of 3D printed laminated composites because of the toughening effect. In addition, the PA-based composites containing both continuous carbon and Kevlar fibers simultaneously tailored rigidity and ductility. Although hybridization of two different fibers significantly enhanced the energy absorption capabilities for hybrid composites compared to non-hybrid composites, the hybrid composites specimens of C-K and K-C exhibited the highest indentation force and total absorbed energy, respectively. The maximum indentation force for C-K was higher than that of K-C, because the Kevlar fibers with high toughness at the rear side of composites might offer an elevated resistance to bear the tensile stresses than carbon fibers. Nevertheless, K-C presented highest total energy absorption capabilities was probably due to K-C showed larger delamination area at outer face of tension side for composites than those of C-K. Thus, the designed position of continuous fiber layers played an important role for energy absorption of the structure.

In current study, we provided a novel concept of printed laminated composites with hybrid continuous fibers. The positive hybrid effects on the designable rigidity and energy absorption capability of the composites were proved by experimental and theoretical approaches. As the mechanical behaviors of the 3D printed laminated composites with continuous fibers highly depend on the printing concepts, the fiber

stacking sequence and fiber content of materials will be investigated in a next study. In addition, the initial defects/interfaces caused by printing strategies have great influences on mechanical behaviors of printed composites. Next work will also focus on the development of analytical and numerical approaches [32-35] with the consideration of initial microstructures for predicting the mechanical behaviors of the 3D printed continuous hybrid fibers reinforced composites.

Acknowledgments: This work was supported by the National Key R&D Program of China (2018YFB1201600), the National Natural Science Foundation of China (No. 51905555 and U1334208), the Hu-Xiang Youth Talent Program (No. 2018RS3002 and 2020RC3009) and the Innovation-Driven Project of Central South University (No. 2019CX017).

Author Contributions: Conceptualization, K.W and Y.P.; data curation and methodology, S.L.; resources, Y.R.; software, Y.W.; writing—original draft, S.L.; writing—review and editing, K.W. and Y.P.

References:

[1] Nizam A, Gopal R, Naing N, Hakim A, Samsudin A. Dimensional accuracy of the skull models produced by rapid prototyping technology using stereolithography apparatus. Archives of Orofacial Sciences. 2006;1:60-6.

[2] Ahn S-H, Montero M, Odell D, Roundy S, Wright PK. Anisotropic material properties of fused deposition modeling ABS. Rapid Prototyping Journal. 2002;8:248-57.

[3] Zhong W, Li F, Zhang Z, Song L, Li Z. Short fiber reinforced composites for fused deposition modeling. Materials Science and Engineering: A. 2001;301:125-30.

[4] Kruth J-P, Mercelis P, Van Vaerenbergh J, Froyen L, Rombouts M. Binding mechanisms in selective laser sintering and selective laser melting. Rapid Prototyping Journal. 2005;11:26-36.

[5] Feygin M, Hsieh B. Laminated object manufacturing (LOM): a simpler process. 1991 International Solid Freeform Fabrication Symposium1991.

[6] Rinaldi M, Ghidini T, Cecchini F, Brandao A, Nanni F. Additive layer manufacturing of poly (ether ether ketone) via FDM. Composites Part B: Engineering. 2018;145:162-72.

[7] Li Q, Zhao W, Li Y, Yang W, Wang G. Flexural Properties and Fracture Behavior of CF/PEEK in Orthogonal Building Orientation by FDM: Microstructure and Mechanism. Polymers. 2019;11:656.

[8] Justo J, Távara L, García-Guzmán L, París F. Characterization of 3D printed long fibre reinforced composites. Composite Structures. 2018;185:537-48.

[9] Rao Y, Wei N, Yao S, Wang K, Peng Y. A process-structure-performance modeling for thermoplastic polymers via material extrusion additive manufacturing. Additive Manufacturing. 2021:101857.

[10] McLouth TD, Severino JV, Adams PM, Patel DN, Zaldivar RJ. The impact of print orientation and raster pattern on fracture toughness in additively manufactured ABS. Additive Manufacturing. 2017;18:103-9.

[11] Wang K, Addiego F, Bahlouli N, Ahzi S, Rémond Y, Toniazzo V. Impact response of recycled polypropylene-based composites under a wide range of temperature: effect of filler content and recycling. Composites Science and Technology. 2014;95:89-99.

[12] Wang P, Zou B, Ding S, Huang C, Shi Z, Ma Y, et al. Preparation of short CF/GF reinforced PEEK composite filaments and their comprehensive properties evaluation for FDM-3D printing. Composites Part B: Engineering. 2020:108175.

[13] Van Der Klift F, Koga Y, Todoroki A, Ueda M, Hirano Y, Matsuzaki R. 3D printing of continuous carbon fibre reinforced thermo-plastic (CFRTP) tensile test specimens. Open Journal of Composite Materials. 2016;6:18-27.

[14] Heidari-Rarani M, Rafiee-Afarani M, Zahedi A. Mechanical characterization of FDM 3D printing of continuous carbon fiber reinforced PLA composites. Composites Part B: Engineering. 2019;175:107147.

[15] Dickson AN, Barry JN, McDonnell KA, Dowling DP. Fabrication of continuous carbon, glass and Kevlar fibre reinforced polymer composites using additive manufacturing. Additive Manufacturing. 2017;16:146-52.

[16] Brooks H, Wright C. Title: 3D printing of continuous Kevlar fibre reinforced composites2019.

[17] Panzera TH, Jeannin T, Gabrion X, Placet V, Remillat C, Farrow I, et al. Static, fatigue and impact behaviour of an autoclaved flax fibre reinforced composite for aerospace engineering. Composites Part B: Engineering. 2020:108049.

[18] Bulut M, Erkliğ A, Yeter E. Hybridization effects on quasi-static penetration resistance in fiber reinforced hybrid composite laminates. Composites Part B: Engineering. 2016;98:9-22.

[19] Thwe MM, Liao K. Effects of environmental aging on the mechanical properties of bamboo–glass fiber reinforced polymer matrix hybrid composites. Composites Part A: Applied Science and Manufacturing. 2002;33:43-52.

[20] Wang K, Li S, Rao Y, Wu Y, Peng Y, Yao S, et al. Flexure Behaviors of ABS-Based Composites Containing Carbon and Kevlar Fibers by Material Extrusion 3D Printing. Polymers. 2019;11:1878.

[21] Peng Y, Wu Y, Li S, Wang K, Yao S, Liu Z, et al. Tailorable rigidity and energy-absorption capability of 3D printed continuous carbon fiber reinforced polyamide composites. Composites Science and Technology. 2020:108337.

[22] Chacón J, Caminero M, Núñez P, García-Plaza E, García-Moreno I, Reverte J. Additive manufacturing of continuous fibre reinforced thermoplastic composites using fused deposition modelling: Effect of process parameters on mechanical properties. Composites Science and Technology. 2019:107688.

[23] Yudhanto A, Wafai H, Lubineau G, Yaldiz R, Verghese N. Characterizing the influence of matrix ductility on damage phenomenology in continuous

fiber-reinforced thermoplastic laminates undergoing quasi-static indentation. Composite Structures. 2018;186:324-34.

[24] Peng Y, Wu Y, Wang K, Gao G, Ahzi S. Synergistic reinforcement of polyamide-based composites by combination of short and continuous carbon fibers via fused filament fabrication. Composite Structures. 2019;207:232-9.

[25] Al-Kinani R, Najim F, de Moura M. The effect of hybridization on the GFRP behavior under quasi-static penetration. Mechanics of Advanced Materials and Structures. 2014;21:81-7.

[26] Al Abadi H, Thai H-T, Paton-Cole V, Patel V. Elastic properties of 3D printed fibre-reinforced structures. Composite Structures. 2018;193:8-18.

[27] Melenka GW, Cheung BK, Schofield JS, Dawson MR, Carey JP. Evaluation and prediction of the tensile properties of continuous fiber-reinforced 3D printed structures. Composite Structures. 2016;153:866-75.

[28] Abisset E, Daghia F, Sun X, Wisnom MR, Hallett SR. Interaction of inter-and intralaminar damage in scaled quasi-static indentation tests: Part 1–Experiments. Composite Structures. 2016;136:712-26.

[29] Abrate S. Impact on composite structures: Cambridge university press, 2005.

[30] Marom G, Fischer S, Tuler F, Wagner H. Hybrid effects in composites: conditions for positive or negative effects versus rule-of-mixtures behaviour. Journal of Materials Science. 1978;13:1419-26.

[31] Bulut M, Erkliğ A. The investigation of quasi-static indentation effect on laminated hybrid composite plates. Mechanics of Materials. 2018;117:225-34.

[32] Wang K, Lu Y, Rao Y, Wei N, Ban J, Peng Y, et al. New insights into the synergistic influence of voids and interphase characteristics on effective properties of unidirectional composites. Composite Structures. 2021;255:112862.

[33] Rouf K, Liu X, Yu W. Multiscale structural analysis of textile composites using mechanics of structure genome. International Journal of Solids and Structures. 2018;136:89-102.

[34] Huang W, Causse P, Hu H, Belouettar S, Trochu F. Transverse compaction of 2D glass woven fabrics based on material twins–Part II: Tow and fabric deformations. Composite Structures. 2020;237:111963.

[35] Huang W, Xu R, Yang J, Huang Q, Hu H. Data-driven multiscale simulation of FRP based on material twins. Composite Structures.256:113013.

Author Contributions:

Conceptualization, K.W and Y.P.; data curation and methodology, S.L.; resources, Y.R.; software, Y.W.; writing—original draft, S.L.; writing—review and editing, K.W. and Y.P.

Conflicts of Interest: The authors declare no conflict of interest.